Competing Crystal Growth in Ge–Sb Phase-Change Films

Gert Eising, Bart-Jan Niebuur, Andrew Pauza, and Bart J. Kooi**

Analysis of crystal growth in thin films of phase-change materials can provide deeper insights in the extraordinary phase transformation kinetics of these materials excellently suited for data storage applications. In the present work crystal growth in Ge_xSb_{100-x} thin films with $x = 6$, 7, 8, 9, and 10 is studied in detail, demonstrating that the crystallization temperature increases from ~80 °C for Ge_6Sb_{94} to ~200 °C for $Ge_{10}Sb_{90}$ and simultaneously the activation energy for crystal growth also significantly increases from 1.7 eV to 5.5 eV. The most interesting new finding is that in the thin films containing 8, 9, and 10 at% Ge two competing growth modes occur which can have several orders of magnitude difference in growth rate at a single external temperature: an initial mode with isotropic slow growth producing circular crystals with smooth surfaces and growth fronts and a fast growth mode producing crystals with triangular shape having rough surfaces and growth fronts indicative of dendritic-like growth. The slow-growth mode becomes increasingly dominant for crystallization at low temperatures when the Ge concentration is increased from 8 to 10 at% Ge. For a certain Ge concentration, the slow growth mode becomes increasingly dominant at lower temperatures and the fast growth mode at higher temperatures. Latent heat produced during crystallization is considered a principal factor explaining the observations. The fast growth mode is associated with (eutectic) decomposition generating more latent heat and instable growth fronts and the slow growth mode is associated with thermodynamically less stable homogeneously alloyed crystals generating less latent heat, but stable growth fronts.

1. Introduction

Crystallization associated with solidification or from supersaturated solutions is omnipresent, playing a central role in materials production (particularly of metals and polymers), but also in geological processes (e.g. solidification of lava),[1] ice formation,[2] biomineralization,[3] etc. Within living systems under special conditions crystals with, for instance, magnetic functionality are formed.[4] Crystallization of amorphous films or marks is important for various applications such as thin film solar cells[5] and rewritable optical disks.[6] Due to the importance of crystallization, the kinetics and morphology of crystal growth have been studied for a long time. Most emphasis has been on crystal growth from the melt or from solutions, where undercooling or supersaturation is the important driver of crystal growth. Crystallization in solid amorphous materials generally requires heating to temperatures above the glass transition temperature and below the melting temperature. Depending on, for example, the sample composition, temperature, contaminations and heating or cooling rates, many crystallization mechanisms leading to various growth rates and morphologies have been observed, for instance planar-front or faceted growth, dendritic growth, spherulitic growth, seaweed growth or growth with dense branching morphology and fractal growth.[7–11] These morphologies largely influence the properties of the crystalline materials, for instance metals and polymers. The present work focuses on phase-change materials which are of importance for data storage applications where their working principle is based on the reversible fast switching of small volumes between amorphous and crystalline phases which show distinct differences in optical and electrical properties.

The pronounced temperature dependence of crystal-growth speed recently found in phase-change materials not only rationalizes their favorable characteristics for non-volatile memory applications, but also suggested new insight into their fundamental properties.[12,13] The kinetic coefficient for crystal growth (which is the limiting growth velocity when the thermodynamic factor is one) was shown to have a non-Arrhenius temperature dependence for the important phase-change material $Ge_2Sb_2Te_5$, indicating a high kinetic fragility of the liquid ($m \approx 90$). Furthermore, there was evidence for substantial decoupling of crystal growth from viscous flow on cooling towards the glass transition temperature T_g: the growth rate extrapolated to T_g was found to be 10^5 times faster than would be calculated from the viscosity of 10^{12} Pa s at the glass transition.[13] Still, this work and other recent work[14] suggest that the growth rate in-between the glass transition temperature and the melting temperature is a continuous function of temperature. Here, we show that this physical picture is in general too simplified. We demonstrate that crystallization in phase-change materials can proceed in different temperature regimes via different growth modes with different temperature dependences of the growth rate. Moreover, in this study we present evidence of crystal growth in amorphous Ge_xSb_{100-x} thin films with $x = 6$, 7, 8, 9, and 10 showing both plane-front

G. Eising, B.-J. Niebuur, Dr. A. Pauza, Prof. B. J. Kooi
Zernike Institute for Advanced Materials
University of Groningen
Nijenborgh 4, 9747AG, Groningen, The Netherlands
E-mail: gerteising@gmail.com; B.J.Kooi@rug.nl

DOI: 10.1002/adfm.201301242

growth and dendritic-like growth at a single external temperature within one sample. Clear evolutions of these competing crystal growth modes are observed as a function of temperature for a certain composition and also as a function of composition *x*. Transition regimes in composition and temperature are found where both crystallization modes proceed at the same time (i.e. for the same composition and temperature). These different modes show different growth rates and morphologies and correspond to different optical contrasts due to the difference in microstructure. The fast growth mode shows a growth mechanism that favorable couples to a crystallization mechanism recently found by molecular dynamics simulations in the phase-change material AgInSbTe.[15]

Crystallization processes, i.e. transformations from amorphous to crystalline phases, are intrinsically exothermic in nature. Inherent to the decrease in entropy upon crystallization and the high crystal growth rates observed for phase-change materials is the probability that explosive crystallization (EC) occurs, implying that the latent heat, released during the initial crystallization induced locally, is used for a self-sustained propagation of the crystallization front. Indeed, EC has been observed in Si, Ge, pure Sb and Sb-alloy films (the latter being of direct importance for PC applications).[16–18] In the alloys from Ge_6Sb_{94} to $Ge_{10}Sb_{90}$ investigated in the present work we did not observe EC for layer thicknesses up to 400 nm. However, this does not mean that latent heat is not produced. Still, latent heat raises the local crystal growth front temperature during crystallization, accelerates crystal growth and contributes to interesting novel crystal growth phenomena presented here.

2. Results

Samples with 200 nm thick phase-change films deposited on glass substrates were placed on a hot plate for isothermal measurements. **Figure 1**a and b show optical recordings taken during isothermal heating at 185 °C of an amorphous Ge_9Sb_{91} film. The crystal nucleation starts after an incubation time of 270 ± 30 s, after which the nucleated crystals grow in a more or less isotropic manner and form crystals with circular shapes, see the inset in Figure 1a. The nucleation rate in these materials is low and only a few additional nuclei are formed during the measurement after the initial nucleation has started. 600 ± 50 s after the annealing temperature has been reached triangular shaped crystals nucleate and start to grow as seen in Figure 1a. Most of these crystals grow at the edge of the already formed round crystals, that is, the already present crystals act as a nucleation sites, but nucleation is also found at new sites in the amorphous film. The triangular shaped crystals have a rougher crystal growth front and show faster crystal growth than the circular crystals. Due to the faster growth of the triangular shaped crystals they grow around the slower circular isotropic growing crystals, see Figure 1b. In time additional fast growth crystals nucleate until the sample is fully crystallized.

The incubation times for both crystal morphologies found in Ge_9Sb_{91} as function of temperature are shown in Figure 1c. For the highest annealing temperature used (188 °C) it was found that only fast growth crystals are visible, as its incubation time has become shorter than or equal to the incubation time for slow growth. For annealing temperatures below 181 °C the sample is fully crystallized by isotropic slow growth within the incubation time pertaining to the fast growth mode, therefore, no fast growth is found.

Time and growth rate mappings, displaying the crystalline-amorphous interface as function of time and the crystal growth rate as function of position, are obtained from the raw images and shown in **Figure 2**a and b.[19,20] From the time mapping (Figure 2a) it can be clearly seen that if the crystalline boundary of the fast growth crosses slow growth, the latter will be embedded in the fast growth crystal with little disturbance in the fast growth crystal boundary once the growth front has passed the slowly growing crystal. In Figure 2b the difference in growth rate between the two crystal growth modes is clearly visible. For example, for T = 185 °C, the slow growth mode crystals grow at a rate of ~0.06 μm s^{-1} while the fast growth shows a growth rate of ~1.1 μm s^{-1}, i.e., almost twenty times faster.

This analysis has been repeated for different temperatures in the range of 180 °C to 188 °C. For each temperature the two most occurring speeds in the histogram of the growth rate mapping have been taken and plotted in an Arrhenius plot, see Figure 2c. Clearly two regimes of growth can be identified, and when fitted using an Arrhenius dependence we obtain two activation energies for growth: 3.0 ± 0.1 eV for the slow growth mode and 6.6 ± 0.2 eV for the fast growth mode. Interesting to note that these crystallization temperatures are very close to the

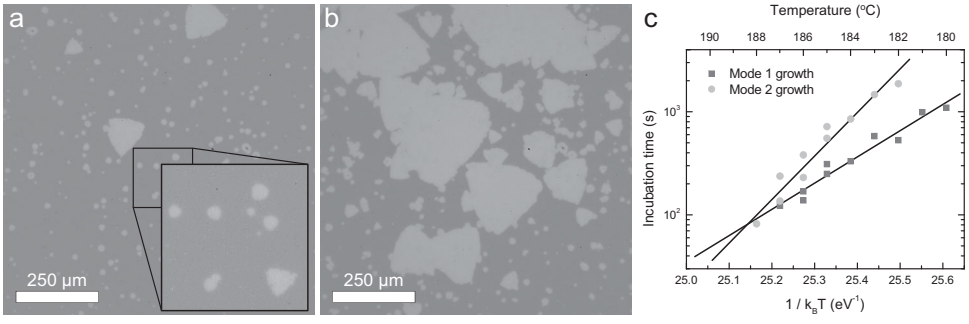

Figure 1. (a,b) Crystal growth as observed in-situ using optical microscopy in a 200 nm thick Ge_9Sb_{91} film at 185 °C: (a) 570 s and (b) 650 s after reaching the isothermal annealing temperature indicating an initial slow growth mode followed by a later fast growth mode. (c) Incubation time for crystallization versus the reciprocal crystallization temperature for the slow (blue squares) and fast (orange circles) crystal growth modes.

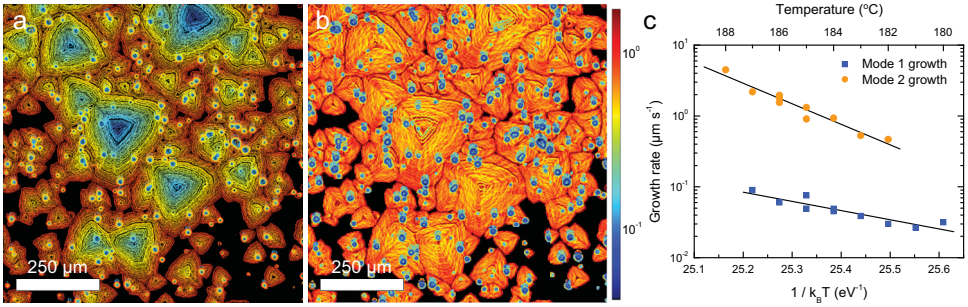

Figure 2. (a) Time mapping of an isothermal experiment at 185 °C for a 200 nm thick Ge_9Sb_{91} film showing the crystalline-amorphous interface as function of time. (b) Crystal growth rate image obtained from the time mapping showing the growth front velocity at each position. (c) Growth rate versus reciprocal temperature for the slow (blue squares) and fast (orange circles) crystal growth modes.

estimated glass transition temperature for Ge_9Sb_{91} of ~181 °C based on calculations by Raoux et al.[21]

A more detailed optical image of both crystal modes is shown in **Figure 3**. From the image it can be clearly seen that the surface of the faster growing triangular shaped crystal is rougher than the isotropic growing crystals, which exhibit a smooth surface. It also shows that there is a difference in height between the crystalline and amorphous phases as expected,[22] but also a difference in height between the two crystalline phases. A dendritic/seaweed-like structure with a threefold symmetric structure can be seen in the fast growing crystals.

Also energy-dispersive X-ray spectroscopy analyses, using a scanning electron microscope, (SEM-EDX) were performed to determine the local chemical compositions of crystals formed by the slow growth mode and the fast growth mode in comparison to the initial amorphous phase. Within the limited excitation volume probed with SEM-EDX in the 200 nm films no relevant composition differences were found between all the phases or morphologies. Figure 2 and 3 may give the impression that the slow and fast growth modes can be associated with phase separation, which may be expected for Ge-Sb alloys, because according to the phase diagram Ge and Sb are hardly miscible and a eutectic occurs at a composition $Ge_{15}Sb_{85}$.[23] However, the SEM-EDX measurements thus clearly indicate that the crystals formed by the slow growth mode or the fast growth mode have the same overall composition equal to the composition of the initial amorphous phase. Moreover, we have another proof that this has to be the case, because both the slow and fast-growth modes can be responsible for the complete crystallization of the phase-change film. The slow growth mode occurs at lower temperatures (≤181 °C) and the fast-growth mode at higher temperatures (≥188 °C) and only at the intermediate temperatures both growth modes occur simultaneously and compete. This is, by itself, a proof that crystals grown by the slow mode cannot be the second phase due to the phase separation, because the second phase alone cannot be responsible for the complete crystallization of the whole film.

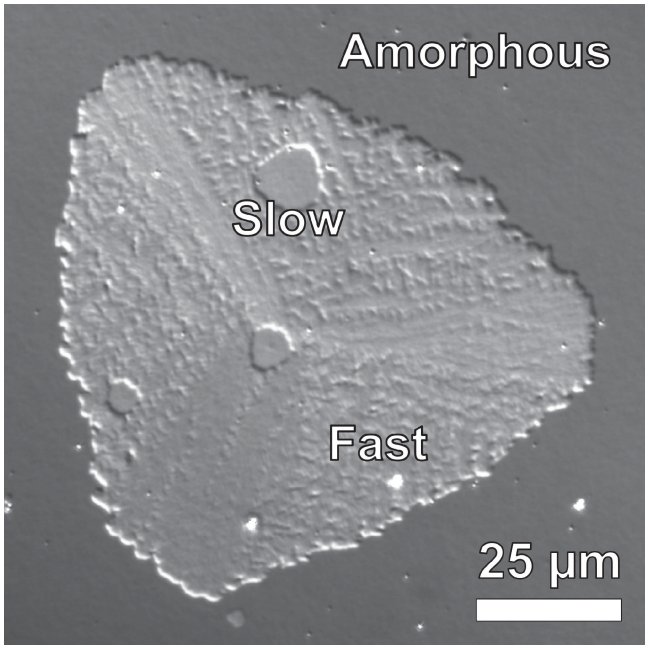

Figure 3. Optical micrograph of a fast mode crystal growing around slow mode crystals in an amorphous background for a 200 nm thick Ge_9Sb_{91} film crystallized at 186 °C.

Interesting results are also obtained when at initial higher temperatures the fast growth mode begins to overtake the slow growth mode after which the temperature is dropped and then growth is recommenced at a slightly lower temperature than the initial one (see supporting information associated with Figure S1). Also at the lower growth temperature again first the slow growth mode precedes the fast growth mode, but with clear differences in morphology and optical reflectivity between the growth modes at the different temperatures.

Experiments, described in detail above for Ge_9Sb_{91} films, were repeated for compositions in the range from Ge_6Sb_{94} to $Ge_{10}Sb_{90}$; see **Figure 4** for an overview of all results. Directly evident from Figure 4 is that the crystallization temperature strongly increases with increasing Ge concentration. Actually this implies that the same crystal growth rate is found for strongly increasing temperatures when the Ge concentration increases, i.e. from about 80 °C for Ge_6Sb_{94} to about 200 °C for $Ge_{10}Sb_{90}$. Moreover, the activation energy for crystal growth is also significantly increasing, i.e., from 1.7 eV for Ge_6Sb_{94} to 5.5 eV for $Ge_{10}Sb_{90}$. For Ge_6Sb_{94} and Ge_7Sb_{93} only a single growth mode is observed. For Ge_8Sb_{92} and $Ge_{10}Sb_{90}$ the same two types of growth modes occur as observed for Ge_9Sb_{91}. However, there is a significant development from Ge_8Sb_{92} to $Ge_{10}Sb_{90}$ as can be seen in Figure 4 and is explained in detail below.

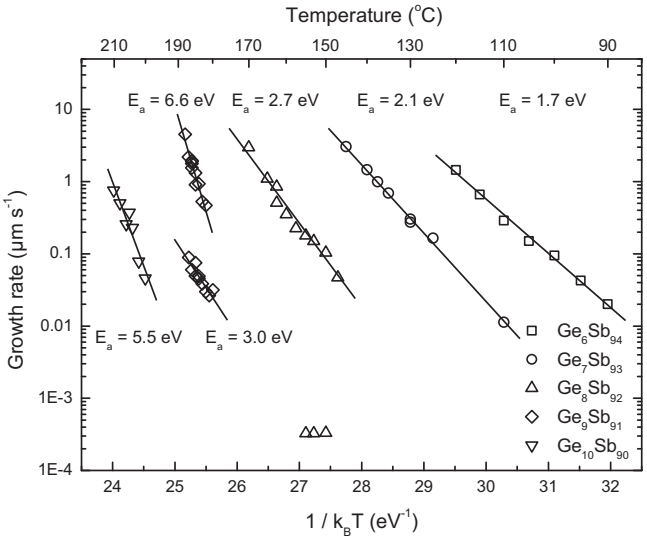

Figure 4. Crystal growth rate as function of temperature for compositions ranging from Ge_6Sb_{94} to $Ge_{10}Sb_{90}$. The black lines are Arrhenius fits to the data points and their slopes provide the indicated values for the activation energies for growth.

For Ge_8Sb_{92} under usual isothermal growth conditions only the fast growth mode is readily observed. In order to detect the slow growth mode first crystals were grown for some limited time with the fast growth mode at 160 °C. Then the temperature was abruptly decreased to about 140 °C after which the sample is heated to temperatures in the range 150–156 °C. At these lower temperatures, still for a relatively long time, the slow growth mode occurs after which a natural (i.e. non-induced) transition to the fast growth mode occurs. An explicit example is shown in **Figure 5**. Upon heating to 160 °C the fast growth mode occurs after an incubation time of ~2 min with a growth rate of 0.4 μm s^{-1}. After cooling to 150 °C the growth mode becomes slow and its growth rate becomes 0.3 nm s^{-1}. Note the more than three orders of magnitude reduction in growth rate when we only cool from 160 °C to 150 °C! After a subsequent incubation time of about 3 hours at 150 °C, during which the slow growth mode occurred, the transition to the fast growth mode occurs leading to a growth rate of 0.1 μm s^{-1}, i.e., again 300 times faster than the rate of the slow growth mode at the same temperature! This procedure resulted in a slow growth mode that does not seem to be thermally activated. It is likely that the procedure to first heat to higher temperatures and then to observe slow growth at lower temperatures primes the amorphous film in such a (relaxed) state that the growth rate of the slow growth mode loses its temperature dependence in this small temperature range.

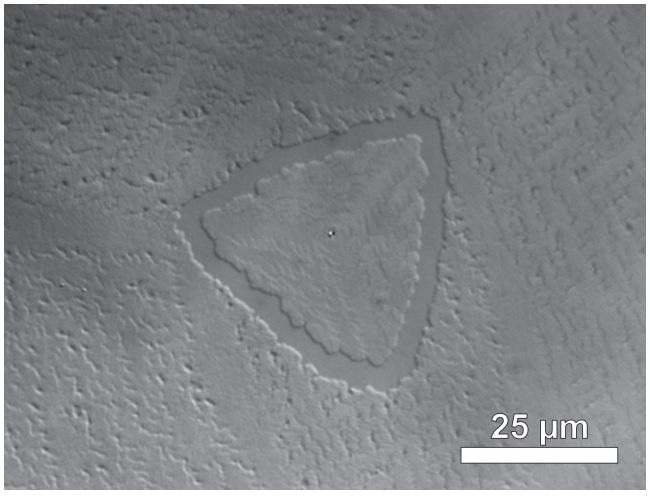

Figure 5. Optical micrograph of the slow and fast crystal growth modes in a 200 nm Ge_8Sb_{92} film. The inner fast growth occurred at 160 °C, the slow growth and outer fast growth at 150 °C.

For $Ge_{10}Sb_{90}$ under usual isothermal growth conditions only the slow growth mode is readily observed. The fast growth mode can be detected, but only after most of the thin film has been crystallized. The remaining amorphous area then has become that small that it prevents a reasonably accurate determination of the growth rate of the fast growth mode. Still it is clear, similar as for Ge_8Sb_{92} and Ge_9Sb_{91}, that the fast growth mode becomes more dominant at relatively higher temperatures and the slow growth mode at relatively lower temperatures. The single growth mode observed for Ge_6Sb_{94} and Ge_7Sb_{93} actually corresponds to the fast growth mode as can be readily deduced from (i) the overall triangular crystal shape, (ii) the dendrite-like structure directly associated with the surface topography and (iii) the observed trends in growth rates when increasing the Ge concentration.

Using transmission electron microscopy (TEM) the crystal structure of the fast growth mode was studied in more detail for 50 nm thick Ge_7Sb_{93} films. The obtained diffraction patterns, with a few examples shown in **Figure 6**, hold for the $R\bar{3}m$ crystal structure that can be described with a hexagonal

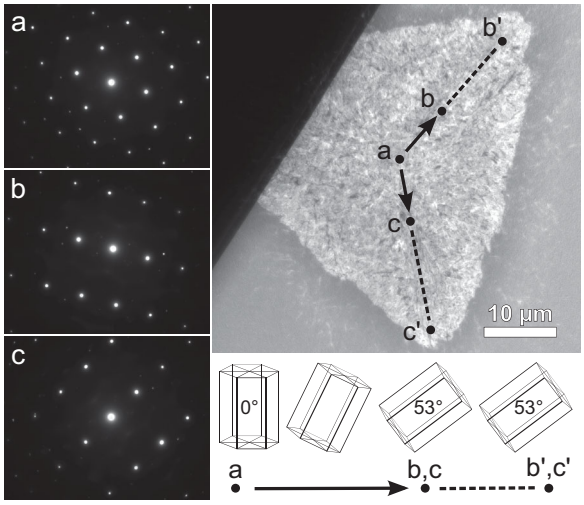

Figure 6. Overview TEM image of a representative crystal with the common triangular shape in a 50 nm thick Ge_7Sb_{93} film where the diffraction patterns are shown for a few decisive locations, i.e., at the center (point a) and along two of the principal growth axes (points b and c). In the center (a) were nucleation occurred the crystal is oriented with the [0001] perpendicular to the surface. Along each growth axis the structure rotates continuously around an axis perpendicular to the growth direction such that the $[20\bar{2}1]$ becomes perpendicular to the surface in b or c and this orientation is maintained during growth to b' or c' as schematically illustrated in the lower right panel.

lattice with a and c lattice parameters of 4.30 ± 0.06 Å and 11.0 ± 0.3 Å, respectively. Diffraction patterns taken at several locations along the growth path, from the center of the crystal (where it actually nucleated) towards the crystal tips at the growth front show a rotation of the crystal structure. In the center, point a in Figure 6, the [0001] axis of the crystal is parallel to the film normal, i.e. crystals tend to nucleate with the (0001) plane parallel to the surface to minimize surface energy.[24,25] However, during subsequent lateral growth of the crystals the crystal orientation at the three tips of the triangular shaped crystals gradually becomes tilted. At a distance of about 7 μm from the center of the crystal the [0001] axis is tilted in the direction of growth with an angle of about 53°, such that the $[20\bar{2}1]$ becomes oriented normal to the film; see point b and c in Figure 6. This tilted orientation appears then to be stable during further lateral growth and the same tilted orientations are found for the points b' and c'. The same result with tilting from the [0001] axis normal to the film in the center of the crystals to the $[20\bar{2}1]$ axis normal to the film at the crystal tips was observed for several crystals analysed with TEM and seems to hold in general for all crystals (with triangular shape) in Ge_7Sb_{93}. Apart from selected area electron diffraction patterns, we also performed TEM-EDX analyses using a probe with a diameter of ~5 nm to measure locally compositions in the crystals (with triangular shape) in Ge_7Sb_{93}. Clear indications of decomposition could not be found, although this cannot be ruled out, because its detection is strongly hampered by the complex (transrotational) structure of the crystals and by the projective nature of the TEM analysis which cannot observe decomposition in the projection direction. Moreover, the type of morphology of these crystals strongly suggests that decomposition on a nanoscale is expected to play a role in contrast to the slow growth mode where crystals are completely homogeneous.

XRD measurements were performed (in Bragg-Brentano geometry) on 400 nm thick Ge_9Sb_{91} films, where one film was completely crystallized (at 180 °C) by the slow growth mode and another was completely crystallized (at 190 °C) by the fast growth mode (see Supporting Information and Figure S2). The results show that the slow growth mode corresponds to a strong texture with the [0001] axis perpendicular to the surface and the fast growth mode results in hardly measurable diffraction peaks, where the (0003) and the $(20\bar{2}1)$ peaks are just discernible. These results consistently explain (in combination with the earlier results) for both growth modes that nuclei develop with the (0001) plane parallel to the surface. However, after nucleation, during lateral growth, transrotational effects are absent for the slow growth mode. For the fast growth mode the presence of strong transrotational effects during growth destruct the diffracted intensity in the (*hkl*) peaks. Still, the weak presence of the (0003) and the $(20\bar{2}1)$ peaks indicate the rotation from [0001] to $[20\bar{2}1]$ perpendicular to the surface as was also observed by TEM for crystals grown by the fast mode in 50 nm thick Ge_7Sb_{93} films.

3. Discussion

All the above results can be casted in a kind of unifying physical picture. We start with the fact that, in the solid state, GeSb alloys are (thermodynamically) not stable in a homogeneous state, because they want to decompose in almost pure Ge and Sb with a eutectic at a composition $Ge_{15}Sb_{85}$. Direct crystallization in such a decomposed (eutectic) state generates most enthalpy. However, at low temperatures, near the crystallization temperature which is also very close to the glass transition temperature (as explained in the previous section), the driving force for crystallization is high, but the atomic mobility very low (viscosity high). Therefore, such decomposition is often suppressed. For pure Sb this does not hold and amorphous Sb already (after some incubation time) crystallizes at room temperature, where also explosive crystallization (EC) can be ignited, indicating the importance of enthalpy release on crystal growth. With increasing Ge concentration, amorphous GeSb becomes stable at room temperature and shows strongly increasing crystallization temperatures as our current work shows when the Ge concentration increases from 6 to 10 at.%. This can be expected, because the more Ge is added to Sb the more crystallization is frustrated.[24,26,27] Also the potential decomposition of the alloy into the pure phases is at low temperatures increasingly frustrated. Therefore, it can be anticipated that below a certain Ge concentration at relatively low temperatures decomposition is still possible and beyond this concentration decomposition is suppressed (but of course decomposition at higher temperatures is still possible in agreement with observations for temperatures beyond 300 °C).[27–29]

The present work shows that the transition in growth mode is not sharp, but that two coexisting growth modes are observed for Ge_8Sb_{92}, Ge_9Sb_{91} and $Ge_{10}Sb_{90}$. The lower temperature branch (slow growth) corresponds to circular crystals with very smooth surfaces and the higher temperature branch (fast growth) to crystals with overall triangular shapes and rough surfaces and crystal-growth fronts indicating dendritic-like growth. The explanation we propose here for these two growth modes is that the dendritic-like mode corresponds to (partial) phase separation such that most latent heat is released during crystallization. In the slow growth mode crystals are formed in which Ge and Sb are still homogeneously alloyed. Because these alloyed crystals exhibit a considerable amount of configurational entropy ($x \ln x + (1 - x) \ln(1 - x)$ in a regular solution model, with x the Ge-concentration), less latent heat is released. In the dendritic-like case the latent heat increases the crystal growth front temperature and provides temperature gradients across the growth-front stimulating this dendritic-like growth. Moreover, impurities are generated which are also considered an important cause for crystal growth front instability.[7,9] In the slow growth mode the lower amount of latent heat released leads to lower growth rates and the absence of decomposition and impurities in combination with the lower growth rate leads to a stable growth front.

The above explanation is consistent with the experimental observations:

1) It explains that with increasing Ge concentration, which increasingly leads to frustration of crystallization and to higher crystallization temperatures, at relatively low temperatures the slow growth mode is introduced and becomes increasingly dominant, because the configurational entropy of the homogeneously alloyed crystal becomes larger, allowing the opening of this new crystal growth branch. The relative increase in configurational entropy for alloyed crystals with

increasing Ge concentration is obvious when considering the $x \ln x + (1-x) \ln(1-x)$ term of a regular solution model (with x the Ge-concentration). It explains why for Ge_8Sb_{92} the fast growth mode is still dominant, that for Ge_9Sb_{91} both growth branches are naturally coexisting and that for $Ge_{10}Sb_{90}$ the slow growth mode becomes dominant (when with normal heating rates isothermal crystallization temperatures are approached showing crystallization after incubation times of typically less than tens of minutes).

2) This explanation is also consistent with the observation that for a certain Ge concentration the fast growth mode is becoming increasingly dominant at higher temperatures and the slow growth mode at lower temperatures, because decomposition is suppressed at the lower temperatures. Moreover, it also explains that a natural transition from the slow to fast growth mode is possible, when still after sufficient time the slow mode is able to produce sufficient latent heat to generate (i) a higher growth front temperature allowing more atomic mobility required for decomposition and (ii) a temperature gradient across the growth-front (with higher temperature ahead of the front in the amorphous phase) such that the growth front loses it stability against perturbations. Then, the transition to the dendritic-like growth mode occurs. On the other hand, a transition from the fast growth mode to the slow growth mode is not directly possible. Only by a decrease in external temperature the fast growth mode can be halted and turned into the slow growth mode, which after a certain incubation time then still at these lower temperatures can switch to the faster growth mode.
3) Obviously, it explains why the faster growth mode is actually faster, but it also partly explains the exceptionally high activation energies for growth found and why this is higher for the fast growth mode. The role played by latent heat is crucial. At higher temperatures with higher growth rates more latent heat per unit of time is produced leading to increasing discrepancies between the actual growth front temperature and the externally applied temperature, where the latter is used for the Arrhenius plots to determine the activation energy for growth. This results in an apparent larger slope (and thus activation energy for growth) in the Arrhenius plots then when the actual growth front temperatures would be used. Note for instance that the temperature interval in Figure 2 used to determine the activation energy for growth for both modes is only 5 K. If the actual temperature interval is 10 K the activation energies for growth would be a factor two lower. Such a relatively subtle additional increase of 5 K for the temperature difference between the lowest and fastest growth rate measured per growth mode can be readily introduced, because the growth rates differ at least a factor three. Note that explosive crystallization can lead to an increase in growth-front temperature, such that a liquid layer is formed at the growth front.[30,31] This is for instance possible for amorphous Si and Ge films.[30,31] Therefore the temperature increases at the growth front proposed in the present work can be considered very modest and highly likely. Moreover, this explanation directly indicates that the activation energies for growth and for overall crystallization determined experimentally have to be considered with care.
4) It explains the difference in growth morphologies observed. The dendrite-like structure can actually be typified as a mixture of a dendrite, seaweed and transrotational crystal structure. Gránásy et al. elegantly showed transitions from single crystal dendritic to polycrystalline seaweed structures.[9] In our case the structure is not single crystalline in the sense of only a translational repeating units in the structure, but it is also not polycrystalline with decoupled orientations of neighboring grains. Actually, during lateral crystal growth also a certain amount of rotation (generally around an in-plane rotation axis tangential to the growth front) couples the newly formed crystal region to the crystal region that was just before at the growth front.[24,32] However, the present transrotational crystals also show important differences with the transrotational crystals found earlier.[24] The earlier ones still showed smooth (apart from the curvature due to the overall shape) planar growth fronts, whereas in the present case the growth fronts are more rough with single or double parabolic tips (see Supporting Information Figure S3), which are typical for dendritic or doublonic growth.[8,10] The transition from dendritic to seaweed growth can have a few origins, such as impurities and reducing the orientational-translational mobility ratio, like nicely demonstrated by the work of Gránásy et al.[9] where the role played by impurities was earlier put forward in Ref.[7] Also in the fast growing crystals, impurities, like introduced intrinsically by the strong driving force for decomposition of the Ge–Sb phase, will contribute to development of the observed mixture of dendritic, seaweed and transrotational crystals. Although there is some disorder in tip splitting and side branching, which is the basis for the seaweed morphology, still images like shown in Figures 3 and 5 clearly indicate that the various branches have preferential mutual orientations (angles) indicative of dendritic growth.

Based on Molecular Dynamics simulations of the phase-change material AgInSbTe (AIST) a proposal for an avalanche-type crystal growth mode was recently put forward.[15] Interestingly, this proposed growth mode appears to couple favorably to the fast growth mode that is observed in the present work. In Ref.[15] a bond-interchange model has been proposed, where crystallization of amorphous AIST can be viewed as a rapid succession of diffusionless events in such a way that the 3+3 octahedra (i.e., with 3 shorter strong bonds and 3 longer weaker bonds also typical for pure Sb) are aligned along the crystalline c axis imposed by the surrounding crystal. Based on reduction of surface (interfacial) energy the crystal nucleus develops with the c axis perpendicular to the surface. Since AIST and the present Ge-Sb alloys are so-called fast-growth type materials having difficulty to nucleate, this favorable orientation is crucial for enabling nucleation. However, this is apparently an unfavorable orientation for growth. Based on the initial symmetry therefore the 3+3 octahedra tend to rotate the c axis in such a way that three main branches develop out of the nucleus with an in-plane mutual angle of 120°. Our work shows that a favorable growth orientation is with the c axis inclined 53° towards the growth direction of each of the three main branches, i.e., the $[20\bar{2}1]$ becomes oriented normal to the film surface. This latter result can of course not be predicted from the bond-interchange model proposed in ref. [15], but the three-fold growth symmetry (cf. Figures 3 and 5) can be understood well on the

basis of this model. The favorable comparison thus holds for the crystallography and the avalanche type crystal growth mode, but a difference is that we expect some nanoscale phase separation between Ge and Sb during the fast growth mode, whereas the bond-interchange model is basically a diffusionless model.

The present explanation thus holds for phase-change materials typified as fast-growth materials (FGM) and in principle only for systems where one or more solutes (like Ge) are added to a solvent (like Sb). However, there is nice analogy with so-called nucleation dominant materials (NDM), typically on or near the GeTe–Sb_2Te_3 tie line. These materials, when crystallized, first form at lower temperatures a meta-stable NaCl-type structure and at higher temperatures a stable trigonal-type crystal structure closely resembling the $R\bar{3}m$ structure of Sb. Although these two crystal growth modes in NDM do not coexist, they correspond to the same solution as found here for FGM, i.e. with two growth modes, where one is forming a more random (higher configurational entropic) system at lower temperatures and the other a more ordered system at higher temperatures. In the meta-stable NaCl type structure, Te atoms are on the Cl-sublattice sites and Ge and Sb are (together with structural vacancies) more or less randomly distributed over the Na-sublattice sites.[33] In the stable rhombohedral crystal structure all the atoms keep their (distorted) octahedrally coordinated position, but Ge and Sb now take an ordered position such that an ordered layered structure is developed. For instance the stable structure of $Ge_2Sb_2Te_5$ can be described by a hexagonal lattice, where the a-b-c stacking of the basal planes in this lattice corresponds to Te-Ge-Te-Sb-Te-Te-Sb-Te-Ge and then repetition of this nine layer basic building block.[34] This clearly demonstrates the more ordered structure at higher temperatures and a more random meta-stable crystal structure at intermediate temperatures. A very similar solution as found here.

The present physical picture can potentially also be related to the observation that the growth rate extrapolated to T_g was found to be 10^5 times faster than would be calculated from the viscosity of 10^{12} Pa s at the glass transition.[13] The reason is that the viscosity is correlated with the actual glass transition temperature, but that the growth rate due to the release of latent heat corresponds to an actually higher temperature at the crystal growth front.

4. Conclusions

Crystal growth has been studied in detail for Ge_xSb_{100-x} thin films with x = 6, 7, 8, 9, and 10 for film thicknesses ranging from 50 to 400 nm. The crystallization temperature increases from about 80 °C for Ge_6Sb_{94} to about 200 °C for $Ge_{10}Sb_{90}$ and simultaneously the activation energy for crystal growth also largely increases from 1.7 eV to 5.5 eV. For Ge_6Sb_{94} and Ge_7Sb_{93} a single growth mode was observed, but in the three alloys with higher Ge concentration two competing growth modes were observed. A slow growth mode produces circular crystals, having smooth crystal growth fronts and surfaces and a fast growth mode produces crystals with a triangular shape, having clearly rougher growth fronts and surfaces corresponding to a growth morphology which is a mixture of dendritic/seaweed/ transrotational growth. Crystals formed by both growth modes have the same overall composition, remaining equal to the initial composition of the amorphous phase. The slow growth mode can only be invoked with difficulty in Ge_8Sb_{92} (and is absent in Ge_6Sb_{94} and Ge_7Sb_{93}), is generally only initially dominant in Ge_9Sb_{91} after which it is overrun by the fast growth mode, but becomes dominant in $Ge_{10}Sb_{90}$, where only in the latest stages of crystallization the fast mode appears. For a certain Ge concentration the slow growth mode is dominant at the lower temperatures and the fast growth mode at higher temperatures, but there is an overlapping temperature interval where the initial slow growth mode is naturally overtaken by the fast growth mode. These observations demonstrate that the common view that the growth rate in-between the glass transition temperature and the melting temperature is a continuous function of temperature is not correct, because there can be orders of magnitude differences in growth rate at a single temperature for the different growth modes. For instance, data retention of phase-change memory is predicted erroneously when measurement data is extrapolated to lower temperatures, but where the growth mode also changes when going to lower temperatures.

Latent heat released upon crystallization is considered a crucial element explaining the above results. In the fast growth mode more latent heat is generated than in the slow growth mode and we attribute this to (partial) decomposition of the GeSb phase in case of fast growth and absence of decomposition in case of slow growth. In this way the growth velocity can be much faster than would be calculated from the viscosity at the external temperature, because latent heat raises the crystal growth front temperature. Also in the present work for Ge_8Sb_{92} orders of magnitude differences in growth rate between the slow and fast growth mode are observed at the same external temperature, which are attributed to differences in enthalpy release and to differences in growth front temperature.

The fast-growth mode observed in the present work shows interesting correspondence with a recently proposed bond-interchange model predicting an avalanche-type crystal growth mode in AgInSbTe phase-change alloys.

5. Experimental Section

Film Preparation: Samples investigated consist of 50, 200, or 400 nm thin films with a $Ge_xSb_{100}x$ composition (with x = 6, 7, 8, 9, and 10) on a 1.3 mm thick glass substrate. The phase-change films were deposited on these substrates simultaneously using co-sputtering with a Unaxis Sputter coater. The deposition rate was 2.5 nm s^{-1}. All the phase-change films were, without breaking the vacuum, directly capped with a 5 nm layer of ZnS-SiO2.

Film Characterization: The topography was measured using a Veeco PicoForce Multimode atomic force microscope (AFM) with Nanoscope V controller. The samples were grounded using silver paste to limit the effect of surface charging on the AFM image. The film compositions were measured locally using Energy-dispersive X-ray spectroscopy (EDAX) connected to an SEM (Philips XL30 FEG-ESEM). TEM was performed using a JEOL2010F operating at 200 kV, where also EDX (Bruker) with a nanoscale (~5 nm) probe was performed to measure compositions on a local scale.

Crystal Growth Characterization: Isothermal measurements were performed on the samples between T = 80 °C and T = 210 °C. These temperatures were chosen for each composition such that the resulting growth rates could be properly recorded in limited time by the optical

technique outlined below. The samples were heated to the desired temperature at a rate of 20 °C min^{-1}. The temperatures were stable within 0.2 °C during the isothermal measurements.

Image Analysis: Crystal growth was observed using a high speed optical camera (Photron 1024 PCI) with zoom objective. The crystal growth rate was obtained quantitatively by analyzing typically 100 to 200 images obtained from the optical recordings. The crystalline areas in the image are determined by first subtracting the amorphous background and removing remaining noise using binary open and close operations. The edges of the crystals are then found using Sobel edge detection. This is done for all recorded images. The edges (amorphous–crystalline interfaces) found in all separate images are combined into one time mapping where the pixels pertaining to each edge receive a value corresponding to the recording time of the image they originated from. Fitting a plane (typically a circle with a radius of 8 pixels) to the non-zero data points around each pixel of the time mapping image gives us the derivative at each pixel, which is direct measure of the inverse growth rate. By inverting each value the crystal growth rate is obtained for each pixel. A growth rate histogram is produced by combining all pixel values for the growth rate. The growth rate pertaining to the most prevalent value in the histogram is considered the relevant growth rate for the crystallization process. This procedure is also explained and applied in refs [19,20].

Supporting Information

Supporting Information is available from the Wiley Online Library or from the author.

Acknowledgements

This research was carried out under project number M62.7.08SDMP03 in the framework of the Industrial Partnership Program on Size Dependent Material Properties of the Materials innovation institute M2i (www.m2i.nl) and the Foundation of Fundamental Research on Matter (FOM) (www.fom.nl), which is part of the Netherlands Organisation for Scientific Research (www.nwo.nl). We gratefully acknowledge XRD measurements and analysis performed by Dr. Graeme Blake.

Received: April 12, 2013
Revised: August 11, 2013
Published online: November 18, 2013

[1] a) S. Labrosse, J. W. Hernlund, N. Coltice, *Nature* **2007**, *450*, 866–869; b) H. B. Mattsson, L. Caricchi, B. S. G. Almqvist, M. J. Caddick, S. A. Bosshard, G. Hetényi, A. M. Hirt, *Nat. Commun.* **2011**, *2*, 299; c) H. S. C. O'Neill, F. E. Jenner, *Nature* **2012**, *491*, 698–704; d) L. Stixrude, N. de Koker, N. Sun, M. Mookherjee, B. B. Karki, *Earth Planet. Sci. Lett.* **2009**, *278*, 226–232.

[2] a) T. Matsunaga, J. Akola, S. Kohara, T. Honma, K. Kobayashi, E. Ikenaga, R. O. Jones, N. Yamada, M. Takata, R. Kojima, *Nat. Mater.* **2011**, *10*, 129–134; b) A. A. Shibkov, Y. I. Golovin, M. A. Zheltov, A. A. Korolev, A. A. Leonov, *Phys. A* **2003**, *319*, 65–79.

[3] a) W. J. E. M. Habraken, J. Tao, L. J. Brylka, H. Friedrich, L. Bertinetti, A. S. Schenk, A. Verch, V. Dmitrovic, P. H. H. Bomans, P. M. Frederik, J. Laven, P. van der Schoot, B. Aichmayer, G. de With, J. J. DeYoreo, N. A. J. M. Sommerdijk, *Nat. Commun.* **2013**, *4*, 1507; b) H. Li, H. L. Xin, M. E. Kunitake, E. C. Keene, D. A. Muller, L. A. Estroff, *Adv. Funct. Mater.* **2011**, *21*, 2028–2034.

[4] a) A. Komeili, Z. Li, D. K. Newman, G. J. Jensen, *Science* **2006**, *311*, 242; b) A. Scheffel, M. Gruska, D. Faivre, A. Linaroudis, J. M. Plitzko, D. Schüler, *Nature* **2006**, *440*, 110–114.

[5] S. Sriraman, S. Agarwal, E. S. Aydil, D. Maroudas, *Nature* **2002**, *418*, 62–65.

[6] a) A. V. Kolobov, P. Fons, A. I. Frenkel, A. L. Ankudinov, J. Tominaga, T. Uruga, *Nat. Mater.* **2004**, *3*, 703–708; b) M. Wuttig, N. Yamada, *Nat. Mater.* **2007**, *6*, 824–832.

[7] a) H. D. Keith, F. J. Padden, *J. Appl. Phys.* **1963**, *34*, 2409–2421; b) N. Goldenfeld, *J. Cryst. Growth* **1987**, *84*, 601–608.

[8] H. M. Singer, J. H. Bilgram, *Phys. Rev. E* **2004**, *70*, 031601.

[9] L. Gránásy, T. Pusztai, T. Börzsönyi, J. A. Warren, J. F. Douglas, *Nat. Mater.* **2004**, *3*, 645–650.

[10] B. Utter, E. Bodenschatz, *Phys. Rev. E* **2005**, *72*, 011601.

[11] B. C. Okerberg, H. Marand, *J. Mater. Sci.* **2007**, *42*, 4521–4529.

[12] M. Wuttig, M. Salinga, *Nat. Mater.* **2012**, *11*, 270–271.

[13] J. Orava, A. L. Greer, B. Gholipour, D. W. Hewak, C. E. Smith, *Nat. Mater.* **2012**, *11*, 279–283.

[14] G. W. Burr, P. Tchoulfian, T. Topuria, C. Nyffeler, K. Virwani, A. Padilla, R. M. Shelby, M. Eskandari, B. Jackson, B.-S. Lee, *J. Appl. Phys.* **2012**, *111*, 104308.

[15] T. Matsunaga, J. Akola, S. Kohara, T. Honma, K. Kobayashi, E. Ikenaga, R. O. Jones, N. Yamada, M. Takata, R. Kojima, *Nat. Mater.* **2011**, *10*, 129–134.

[16] D. A. Kurtze, W. van Saarloos, J. D. Weeks, *Phys. Rev. B* **1984**, *30*, 1398–1415.

[17] M. O. Thompson, G. J. Galvin, J. W. Mayer, P. S. Peercy, J. M. Poate, D. C. Jacobson, A. G. Cullis, N. G. Chew, *Phys. Rev. Lett.* **1984**, *52*, 2360–2363.

[18] C. E. Wickersham, G. Bajor, J. E. Greene, *Solid State Commun.* **1978**, *27*, 17–20.

[19] J. L. M. Oosthoek, B. J. Kooi, J. T. M. De Hosson, R. A. M. Wolters, D. J. Gravesteijn, K. Attenborough, *Microsc. Microanal.* **2010**, *16*, 291–299.

[20] G. Eising, A. Pauza, B. J. Kooi, *Cryst. Growth Des.* **2013**, *13*, 220–225.

[21] S. Raoux, M. Salinga, J. L. Jordan-Sweet, A. Kellock, *J. Appl. Phys.* **2007**, *101*, 044909.

[22] W. K. Njoroge, H.-W. Woltgens, M. Wuttig, *J. Vac. Sci. Technol., A* **2002**, *20*, 230–233.

[23] R. W. Olesinski, G. J. Abbaschian, *Bull. Alloy Phase Diagrams* **1986**, *7*, 219–222.

[24] B. J. Kooi, J. T. M. De Hosson, *J. Appl. Phys.* **2004**, *95*, 4714–4721.

[25] A. K. Petford-Long, R. C. Doole, C. N. Afonso, J. Solís, *J. Appl. Phys.* **1995**, *77*, 607.

[26] M. H. R. Lankhorst, *J. Non-Cryst. Solids* **2002**, *297*, 210–219.

[27] S. Raoux, C. Cabral, L. Krusin-Elbaum, J. L. Jordan-Sweet, K. Virwani, M. Hitzbleck, M. Salinga, A. Madan, T. L. Pinto, *J. Appl. Phys.* **2009**, *105*, 064918.

[28] T. Okabe, S. Endo, S. Saito, *J. Non-Cryst. Solids* **1990**, *117–118*, Part 1, 222–225.

[29] L. Krusin-Elbaum, D. Shakhvorostov, C. Cabral, S. Raoux, J. L. Jordan-Sweet, *Appl. Phys. Lett.* **2010**, *96*, 121906.

[30] H.-D. Geiler, E. Glaser, G. Götz, M. Wagner, *J. Appl. Phys.* **1986**, *59*, 3091–3099.

[31] a) C. Grigoropoulos, M. Rogers, S. H. Ko, A. A. Golovin, B. J. Matkowsky, *Phys. Rev. B* **2006**, *73*, 184125; b) L. Nikolova, T. LaGrange, M. J. Stern, J. M. MacLeod, B. W. Reed, H. Ibrahim, G. H. Campbell, F. Rosei, B. J. Siwick, *Phys. Rev. B* **2013**, *87*, 064105.

[32] V. Yu. Kolosov, A. R. Thölén, *Acta Mater.* **2000**, *48*, 1829–1840.

[33] a) T. Nonaka, G. Ohbayashi, Y. Toriumi, Y. Mori, H. Hashimoto, *Thin Solid Films* **2000**, *370*, 258; b) N. Yamada, T. Matsunaga, *J. Appl. Phys.* **2000**, *88*, 7020.

[34] a) B. J. Kooi, J. T. M. De Hosson, *J. Appl. Phys.* **2002**, *92*, 3584–3590; b) J. Kim, J. Kim, S.-H. Jhi, *Phys. Rev. B* **2010**, *82*, 201312.